Theoretical and Applied Fracture Mechanics 119 (2022) 103325

Contents lists available at ScienceDirect

Theoretical and Applied Fracture Mechanics

journal homepage: www.elsevier.com/locate/tafmec

Tensile mode fracture toughness experiments on andesite rock using disc and semi-disc bend geometries with varying loading spans

Levent Tutluoglu [a], Ceren Karatas Batan [a], M.R.M. Aliha [b,*]

[a] Department of Mining Engineering, Middle East Technical University, Ankara, Turkey
[b] Welding and Joining Research Center, School of Industrial Engineering, Iran University of Science and Technology (IUST), Narmak, 16846-13114 Tehran, Iran.

ARTICLE INFO

Keywords:
Ankara andesite rock
Mode I fracture toughness
Three-Point bending
Disc and semi-disc core-based specimens
Geometry and loading span effect
Maximum tangential strain criterion

ABSTRACT

Purpose of this research is to investigate the effect of loading span on mode I fracture toughness for tests conducted by three-point bend geometries. Mode I fracture toughness tests were conducted on Ankara Golbasi Andesite with straight notched disc bending (SNDB) specimens of thicknesses 50 mm and 60 mm. Loading spans were varied in a wide range between 40 mm and 90 mm corresponding to span/radius ratios of $S/R = 0.40$ to 0.90. Three-point bend tests were conducted with the semi-circular bending (SCB) core specimen geometry for comparison purposes. Mode I fracture toughness results for tests with 60 mm and 50 mm thick SNDB specimens were about 30% greater than the results of SCB tests. It was found that mode I fracture toughness, K_{Ic} increases with decreasing the span length for both SNDB and SCB specimens. Mode I fracture toughness values was also increased with increasing the specimen thickness for the SNDB geometry. The differences in K_{Ic} results of different specimen geometries were explained by a mechanism employing maximum normal strain criterion. It was demonstrated that despite the dependency of critical stress intensity factor to the geometry and loading conditions of the tested specimen, the critical value of maximum tangential strain ($\varepsilon_{\theta\theta c}$) at the onset of fracture is a material constant and its value is nearly the same for all disc and semi-disc geometries tested with varying loading spans.

1. Introduction

Fracture toughness is a parameter for controlling a particular material's crack resistance under a specific loading condition. Mode I loading condition is an important phenomenon in rock fracture mechanics, since brittle rocks are weak under tension. International Society for Rock Mechanics (ISRM) suggests some methods to assign rock fracture toughness for mode I (K_{Ic}). The methods of the short rod [1], chevron bend [2], cracked chevron notched Brazilian disc [3,4] and semi-circular bending [5-7] are some of them. Performing fracture toughness tests with some of these methods can be difficult owing to the sample preparation and the testing procedures. The mode I fracture toughness of the rocks can be measured in a simpler way by using core specimens [8-10]. Cores are readily available from borehole investigations. Applicability of core disc test specimens and their performance for determining K_{Ic} are challenging areas in rock fracture mechanics, since specimen size is restricted with specimen thickness and core diameter [11].

Two simple core specimen geometries and testing methods are adapted in this research. Pure tensile mode fracture tests are conducted with straight-notched disc bending (SNDB) specimen and semi-circular disc bend (SCB) specimen to measure K_{Ic} of the rocks. In both specimens the loading is applied by three-point bending of the discs and these two specimens were widely used for investigation of fracture of geomaterials [12-15]. Tutluoğlu and Keles [16], introduced the SNDB specimen geometry and performed mode I fracture toughness tests on andesite. Wei et al. [17] used the same geometry but with chevron notch type crack for conducting pure mode I fracture toughness on granite and sandstone rock materials. Mixed mode loading was taken into account by varying the crack inclination angle of edge notched disc bending (ENDB) geometry or changing the location of loading supports [14,15,18-32] which is essentially the same geometry as SNDB.

Specimen geometry, material type, crack type and loading condition may have significant effects on the value of the mode I fracture toughness. A large number of experimental, theoretical, and numerical modeling research works have been performed in the past to analyze such effects on the mode I fracture toughness. For example, The influence of specimen shape was studied by using center cracked Brazilian disc (BD) and SCB specimens of Guiting Limestone by Aliha et al. [33].

* Corresponding author.
E-mail address: mrm_aliha@iust.ac.ir (M.R.M. Aliha).

https://doi.org/10.1016/j.tafmec.2022.103325
Received 9 January 2022; Received in revised form 2 March 2022; Accepted 15 March 2022
Available online 18 March 2022
0167-8442/© 2022 Elsevier Ltd. All rights reserved.

Nomenclature

List of Symbols

a	Crack length
t	Specimen thickness
R	Specimen radius
D	Specimen diameter
S	Half-Span length
σ	Normal stress
P	Applied load
P_f	Applied load at fracture
σ_t	Tensile strength
Y_I	Dimensionless stress intensity factor
K	Stress intensity factor
K_{I}	Mode I stress intensity factor
K_{II}	Mode II stress intensity factor
K_{III}	Mode III stress intensity factor
K_c	Fracture toughness
K_{Ic}	Mode I fracture toughness
J	J integral
ν	Poisson's ratio
E	Young's modulus
R	Distance from crack tip
r_c	Critical distance
$\sigma_{\theta\theta}$	Tangential stress
$\varepsilon_{\theta\theta}$	Tangential strain
$\varepsilon_{\theta\theta c}$	Critical tangential strain

Abbreviations

LEFM	Linear elastic fracture mechanics
CCNBD	Cracked chevron notched Brazilian disc method
CNSCB	Chevron-notched SCB method
SR	Short rod method
CB	Chevron bend method
SCB	Semi-Circular bending method
SNDB	Straight notched disc-bending method
ENBD	Edge notched disc bend method
ENDC	Edge notched diametrically compressed method
CNBB	Chevron notched bend beam
CCNSCB	Cracked chevron notched semicircular bending method
NSCB	Notched semi-circular bend method
ISENB	Inclined single-edge-notched beam specimen
SENB	Inclined single-edge-notched beam specimen
CB	Chevron bend
SECRBB	Single edge cracked round bar bend
SCCBD	Straight center cracked Brazilian disc
HMA	Hot mix asphalt mixtures
SMA	Stone mastic asphalt mixtures
SIF	Stress intensity factor
UCS	Uniaxial compressive strength
ISRM	International Society for Rock Mechanics and Rock Engineering
FPZ	Fracture process zone

Mode I fracture toughness tests were performed on the SCB specimens made of Guiting Limestone with crack lengths of 15 mm and 30 mm in that work [33] but the crack length of the BD specimen was set as 15 mm. The average fracture toughness of the BD specimens was two-thirds of the SCB specimen with $a = 30$ mm. Aliha et al. [34], performed mode I fracture toughness tests on hot mix asphalt (HMA) mixtures with ENDB and edge notched diametrically compressed (ENDC) specimen geometries. K_{Ic} of ENDB specimen geometry was about 15% greater than the corresponding K_{Ic} value of ENDC specimen geometry. Aliha et al. [35], conducted mode I fracture toughness tests on Harsin marble with ENDB and inclined single-edge-notched beam (ISENB) specimen geometries. K_{Ic} of ENDB specimen geometry was about 4% larger than K_{Ic} value of beam specimen geometry under pure mode I. Six different specimen geometries were used by Aliha et al. [36], for mode I fracture toughness tests on Harsin marble. K_{Ic} of chevron notched bend beam (CNBB) and single edge notched beam (SENB) tests were found to be larger than 1.405 MPa$\sqrt{\mathrm{m}}$. K_{Ic} results for the other four specimen geometries were ordered as 1.405MPa$\sqrt{\mathrm{m}}$ > chevron bend (CB) > single edge cracked round bar bend (SECRBB) > cracked chevron notched Brazilian disc (CCNBD) > straight center cracked Brazilian disc (SCCBD). In Wei et al. [37], it was found that the average K_{Ic} results of the CCNSCB were higher than the NSCB tests results for the same specimen size. K_{Ic} results of the CCNSCB and NSCB specimens was increased by 20% with increasing radii from 25 mm to 75 mm. In another research work Wei et al. [38], used 25, 50 and 75 mm diameter CCNBD and cracked chevron notched semicircular bending (CCNSCB) specimens for fracture toughness tests on Changtai granite. K_{Ic} results of the CCNBD specimens were 36%, 38% and 34% lower than the results with CCNSCB specimens of radii 25, 50, and 75 mm, respectively. Chang et al. [39], employed CCNBD (cracked chevron-notched Brazilian disc) specimens with 75 and 54 mm in diameter and 15–35 mm in thickness to investigate the effect of specimen size on fracture toughness. For tests on the SCB specimens of granite and marble, K_{Ic} values were scattered for various notch lengths (a/D = 0.07–0.40) and showed no significant trends. In Ref. [40], the average K_{Ic} value of SCB tests was 0.68 MPa$\sqrt{\mathrm{m}}$ for granite, which was 50% lower than the value from the CCNBD tests. K_{Ic} was 0.87 MPa$\sqrt{\mathrm{m}}$ for marble which was 18% lower than the value obtained from the CCNBD tests. The reason was attributed to the lack of pre-cracking in their tests, considering that a sharp crack like in chevron-notched specimens is forced to go through strong grains and more energy is required for cross-grain crack propagation. Tests with chevron-notched SCB specimens (CNSCB) were yielded mode I fracture toughness values very close to those from ISRM suggested CCNBD tests. From the CNSCB test, the corresponding values of K_{Ic} were determined about 1.39 and 1.11 MPa$\sqrt{\mathrm{m}}$, respectively for granite and marble [40].

Haghighatpour et al. [41], presented results of mode I fracture toughness tests on asphalt mixtures with the ENDB specimens. The thicknesses of ENDB specimens were 35, 50 and 65 mm in Ref. [41] to investigate the effect of specimen size on fracture toughness. The average fracture toughness of asphalt mixtures increased up to 2.5 times when the ENDB specimen thickness was increased from 35 mm to 65 mm. Aliha and Haghighatpour [42] performed mode I and mode III fracture toughness tests on hot mix asphalt (HMA) using the ENDB specimen with thickness of 35, 50 and 65 mm. Based on their results the mode I and mode III fracture toughness values were increased with increasing the specimen thickness from 35 to 65 mm. By testing gypsum material using three-different diametral compressed cracked disc configurations, Aliha and co-workers [43] showed that the fracture toughness value depends on the type of test sample and up to 10% discrepancy was observed in the measured K_{Ic} value of gypsum. Some other researchers presented results of mode I fracture toughness tests using bend beam specimens [36,37]. Wei and Dai [44], conducted fracture tests on saline ice beam specimens under mode I loading. Tang et al. [45] also performed fracture tests on notched granite beams under three-point bending.

Limited investigations on the effect of loading span length (used with three-point bend specimen geometries) on mode I fracture toughness is seen in the previous works. In Chong et al. [46], the span length was set as S/R = 0.80 for fracture tests on shale with the SCB geometry. The average fracture toughness was 0.85 MPa$\sqrt{\mathrm{m}}$. Singh and Sun [47],

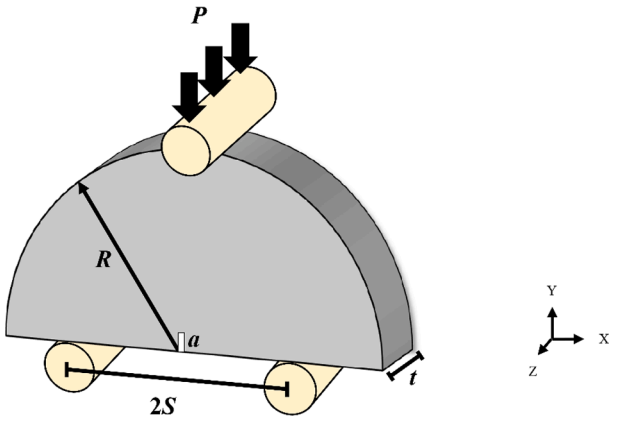

Fig. 1. The semi-circular bend (SCB) specimen.

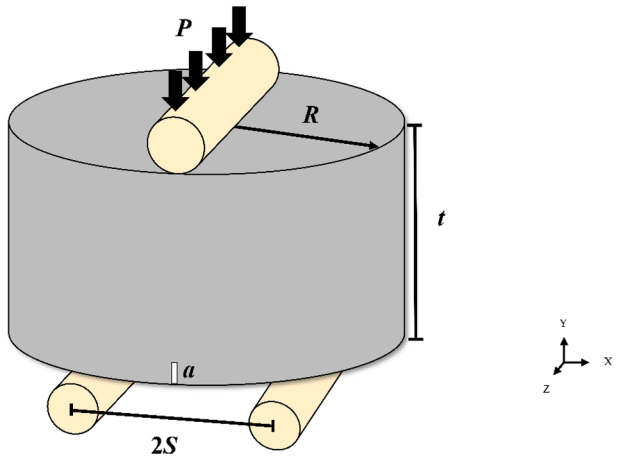

Fig. 2. The single notch disc bend (SNDB) specimen.

conducted fracture tests on welsh limestone with the SCB specimen geometry to measure the mode I fracture toughness. The span length was set as $S/R = 0.80$ in that work. The average fracture toughness value was 1.02 MPa$\sqrt{\text{m}}$. Also, in fracture tests performed by Khan and Al-Shayea [48] with the SCB specimen geometry, the span length was set as $S/R = 0.82$. Wong et al. [49], conducted mode I fracture toughness tests on Kowloon granite using the SCB specimen. The span length of the SCB specimen geometry was set as $S/R = 0.62$ and the corresponding value of average fracture toughness was 1.24 MPa$\sqrt{\text{m}}$. In Eghbali et al. [20], the span length of the ENDB specimen geometry was set equal to $S/R = 0.80$ and the K_{Ic} value was 0.98 and 0.79 MPa$\sqrt{\text{m}}$ for HMA and SMA mixtures, respectively. In a similar work published by Bidadi et al. [50], the span length of the ENDB specimen geometry was set as $S/R = 0.95$ and the mode I fracture toughness value of the tested marble was 2.208 MPa$\sqrt{\text{m}}$. Du et al. [51], conducted fracture tests using the CCNSCB specimens. The span length was set as $S/R = 0.30$, 0.5 and 0.8. It was observed that the critical cracks are highly loading rate-dependent for specimens with smaller support spans. Dealing with the loading rate dependency Xu et al. [52], set the span length of the NSCB specimen as $S/R = 0.5$ under mode I loading condition. They observed that fracture toughness increases with increasing the loading rate. In the work of Lim et al. [53], results of fracture toughness tests on Jhonstone using the SCB specimen geometry were reported. The span length was set as $S/R = 0.50$ and 0.80. The average fracture toughness was 0.06 MPa$\sqrt{\text{m}}$ and no significant effect of the loading span ($2S$) on K_{Ic} was observed. In the work of Tutluoglu and Keles [16], the span length of the SCB and SNDB specimen geometries was set as $S/R = 0.60$ and 0.70 for andesite rock material. No significant effect of the loading span ($2S$) on K_{Ic} was observed but span ranges used in their work were limited anyhow.

As reviewed above, range of spans used for three-point bending tests is limited. Varying the loading span in a wide range is attractive to investigate its effect on K_{Ic}. In the present study with two core-based specimen geometries, investigation of the effect of varying loading span on K_{Ic} is carried out. SNDB and SCB geometries under three-point bending are used with extremely narrow and extremely large spans. In addition for employing a wide range of spans, a span of $S/R = 0.40$ which has been used rarely before in three-point bending configurations is employed in some of the tests. Another aim is to observe the effect of changing the thickness of sample on K_{Ic} for the SNDB geometry.

2. Core-based three-point bend test samples

In three-point bend tests, size independent tensile mode fracture toughness is being tried to reach, suffering minimum from fracture process zone ahead of the crack tip. The well-known core-based ISRM suggested semi-circular bending (SCB) method [5,6], is chosen for the comparison purposes. The SCB specimen proposed by Chong and Kuruppu [5], is illustrated in Fig. 1.

In Fig. 1, *P, 2S, t, a,* and *R* refer to the applied load, span length, thickness, notch length, and radius of the specimen, respectively. The K_{Ic} is computed by below expression:

$$K_{Ic}(SCB) = Y_I(SCB)\sigma_{cr}\sqrt{\pi a} \tag{1}$$

where;

$Y_I(SCB)$ = dimensionless stress intensity factor of SCB specimen.

$\sigma_{cr} = (P_{cr}/2Rt)$

P_{cr} = load at fracture.

The straight notched disc bending specimen was developed by Tutluoglu and Keles [16]. This method was later adopted, improved and the specimen geometry was named as edge notched disc bend (ENDB) [20,22]. The suggested three-dimensional specimen geometry with circular plate type is inherently stiffer than normal specimen geometries with beam type [16]. The specimen geometry is illustrated in Fig. 2.

In Fig. 2, *P, 2S, t, a, R* refer to the applied load, span length, thickness, notch length and radius of the specimen, respectively. The corresponding value of K_{Ic} using this specimen is computed by expression below:

$$K_{Ic}(SNDB) = Y_I(SNDB)\sigma_{cr}\sqrt{\pi a} \tag{2}$$

where;

$Y_I(SNDB)$ = Dimensionless stress intensity factor of SNDB specimen.

$\sigma_{cr} = (P_{cr}/2Dt)$

P_{cr} = load at fracture.

D = disc diameter.

3. Numerical modeling of three-point bend specimen geometries

Numerical computation of stress intensity factor (SIF) in the models was done by ABAQUS finite element program. ABAQUS software package uses the J- integral method to analyze the stress field near the crack tip. J-integral, which is path independent contour integral around the crack tip, is used to calculate the stress intensity factor. Both SNDB and SCB specimens were modeled in the ABAQUS using 3D simulations. Loading span lengths were varied between $S/R = 0.40$–0.90. The crack length was fixed as 10 mm resulting in $a/R = 0.20$ for both geometries. The span length was set as $2S = 40$, 45, 50, 55, 60, 70, 80, 85 and 90 mm. In the modeling work, seam crack length of 10 mm is used for all models in general. The reason for selecting a rather small crack length can be explained by testing work practice. Size effect and FPZ (Fracture Process Zone) are to be minimized by having a small crack relative to the overall specimen size. Load readings are expected to be relatively high, reducing the load-measurement system errors. Smaller cracks reduce the geometry dependence of K_{Ic} measurements. A finer mesh is constructed

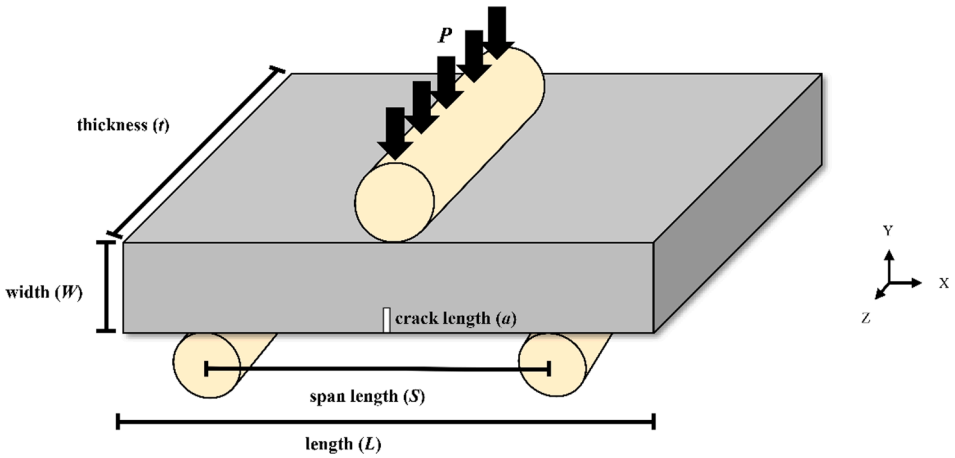

Fig. 3. Geometry of three-point bending plate model.

around the crack tip. Three different partition circles are used to define the contour integral region. The ratio between the contour integral region radius and model geometry radius is set to 0.1 for the SNDB and SCB specimen geometries [16]. The outermost radius of the contour integral region is set as 5 mm for the SCB and SNDB specimen geometries. The intermediate and the innermost radius of the contour integral region are set as 3.5 mm and 0.25 mm, respectively. The area occupied by the innermost radius of the contour integral region is meshed by the hex-dominated element type with sweep technique. For all modeling work in general, a vertical compressive unit line load of −1N is applied to the upper boundary from a reference point above the boundary. The reference point converts the concentrated load to a distributed load at the upper boundary.

3.1. Verification work for the modeling procedure

To assess the accuracy of the stress intensity factor computation of ABAQUS 3D modeling for the SNDB specimen geometry, two problems for which analytical solutions are available are chosen. Verification work involves 3D modeling of well-known Srawley problem for which an analytical soltion exists and the SCB problem for which a semi-analytical solution exists.

3.1.1. Three-point bending plate problem

The numerical model of the three-point bending plate (Fig. 3) is constructed with three steel rollers and one plate loaded by three-point bending of the rollers. a/W and S/a ratios are taken to be equal to 0.5 and 8, respectively. The roller diameter is assigned as 10 mm. The material properties of the steel rollers are elastic modulus (E) = 200 GPa and Poisson's ratio (ν) = 0.30.

Mode I stress intensity factor (K_I) was computed as 738.49 $Pa\sqrt{m}$ as the result of modeling. A polynomial expression was developed by Srawley [54], to calculate the stress intensity factor for a square plate under plane strain condition. The function f(a/W) and stress intensity factor formulas were expressed in Equations (3) and (4) for $0 \le \alpha/W \le 1$.

$$f\left(\frac{a}{W}\right) = 3\left(\frac{a}{W}\right)^{1/2}\left[\frac{1.99 - \left(\frac{a}{W}\right)\left(1-\frac{a}{W}\right)\left(2.15 - \frac{3.93a}{W} + \frac{2.7a^2}{W^2}\right)}{2\left(1+\frac{2a}{W}\right)\left(1-\frac{a}{W}\right)^{\frac{3}{2}}}\right] \tag{3}$$

$$K_I = \frac{P^*S^*f\left(\frac{a}{W}\right)}{tW^{\frac{3}{2}}} \tag{4}$$

where a is the crack size, S is the span length of Srawley beam, W is the width and t is the thickness.

The mode I stress intensity factor (K_I) is calculated as 752.36 $Pa\sqrt{m}$ analytically. The discrepancy between the numerical and analytical solution is 1.88%. It should be noted that the numerical solution is 3D-based while the analytical solution is 2D-based under plane strain assumption.

Table 1
Geometrical dimensions of the SCB models.

Description	Values
Specimen thickness, t (mm)	50
Span length, S (mm)	20, 22.5, 25, 27.5, 30, 35, 40, 42.5, 45
a/R	0.20
S/R	0.40, 0.45, 0.50, 0.55, 0.60, 0.70, 0.80, 0.85, 0.90

3.1.2. Modeling of the SCB specimen

Second verification example is the modeling of well-known and ISRM suggested SCB specimen geometry under three-point bending. The results from the analytical solutions and numerical solutions are compared. 100 mm diameter SCB geometries with 50 mm thicknesses ($t/R = 1$) are modeled. Load is transferred to the model geometry by a reference point. Bottom support lines are fixed vertically in y-direction and set free in horizontal x-and z-directions. This generates a frictionless contact condition between the specimen and the rollers. In fact, support rollers were free to move laterally in testing. The span length is set as $2S$ = 40, 45, 50, 55, 60, 70, 80, 85, and 90 mm. Nine different geometries are modeled in 3D conditions to compute the SIFs of the SCB. The model dimensions of the SCB specimen geometry are listed in Table 1.

The dimensionless stress intensity factor (Y_I) of the SCB model geometry for mode I is formulated by the following equation:

$$Y_I = \frac{K_I}{\sigma_0\sqrt{\pi a}} \tag{5}$$

where K_I is the mode I stress intensity factor and a is the crack length, $\sigma_0 = P/2Rt$ is the stress distributed to the flat bottom, P is the applied load, R is the radius, and t is the thickness of the SCB specimen. Semi-analytical solution for computing Y_I of the SCB geometry is given by Lim et al. [55]. The solution is based on the plane strain assumption. Lim et al. [55], tabulated the dimensionless stress intensity factors for varying a/R and S/R. Results from these tables are adopted for the entries of crack length/radius ratio of $a/R = 0.20$ and span length/radius ratios of 0.50 and 0.80.

Y_I results of the SCB geometry computed from Lim et al. [55], are 2.51 and 4.59 for $S/R = 0.50$ and 0.80, respectively. Modeling work here yields 2.53 and 4.62 for the relevant loading spans. Results are close with differences around 1%. It should be noted that results of this work are from 3D modeling instead of plane strain solutions. Graphical

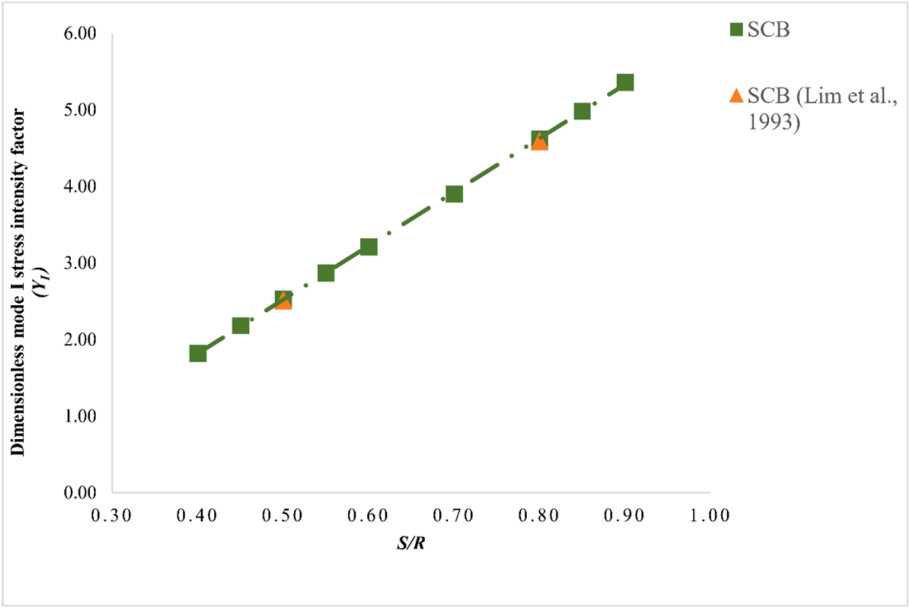

Fig. 4. Dimensionless mode I SIF versus S/R for the SCB specimen.

Table 2
Geometrical dimensions of the SNDB models.

Description	Values
Specimen thickness, t (mm)	50, 60
Span length, S (mm)	20, 22.5, 25, 27.5, 30, 35, 40, 42.5, 45
S/R	0.40, 0.45, 0.50, 0.55, 0.60, 0.70, 0.80, 0.85, 0.90
t/R	1.0, 1.2

illustration of the Y_I versus span length S/R of the SCB from numerical models and Lim's equations are shown in Fig. 4.

Data processing yields a linear relation for the variation of Y_I with S/R. For estimating the dimensionless mode I stress intensity factor of the SCB model geometries, the following equation is proposed for different loading spans:

$$Y_{I(SCB)} = 7.032\left(\frac{S}{R}\right) - 0.996 \text{for} \frac{t}{R} = 1.0 \tag{6}$$

This relation is important in the sense that Y_I results here are from an accurate 3D modeling.

3.2. Modeling of the SNDB specimen

SNDB (straight-notched disc bending) specimen geometry was modeled in 3D condition. Loading span lengths were varied between $S/R = 0.40$–0.90. In the SNDB simulations, 100 mm diameter with 50 mm and 60 mm thicknesses ($t/R = 1$ and $t/R = 1.2$) were modeled without rollers. Load is transferred to the model by a reference point at the top. Bottom support lines are fixed vertically and set free in horizontal x- and z- directions. The span length is set as $2S = 40$, 45, 50, 55, 60, 70, 80, 85 and 90 mm. Eighteen different 3D geometries are modeled to compute the SIF of the SNDB. The model dimensions of the SNDB specimen geometry are listed in Table 2.

The dimensionless stress intensity factor (Y_I) of the SNDB model geometry for mode I is formulated by the following equation:

$$Y_I = \frac{K_I}{\sigma_0\sqrt{\pi a}} \tag{7}$$

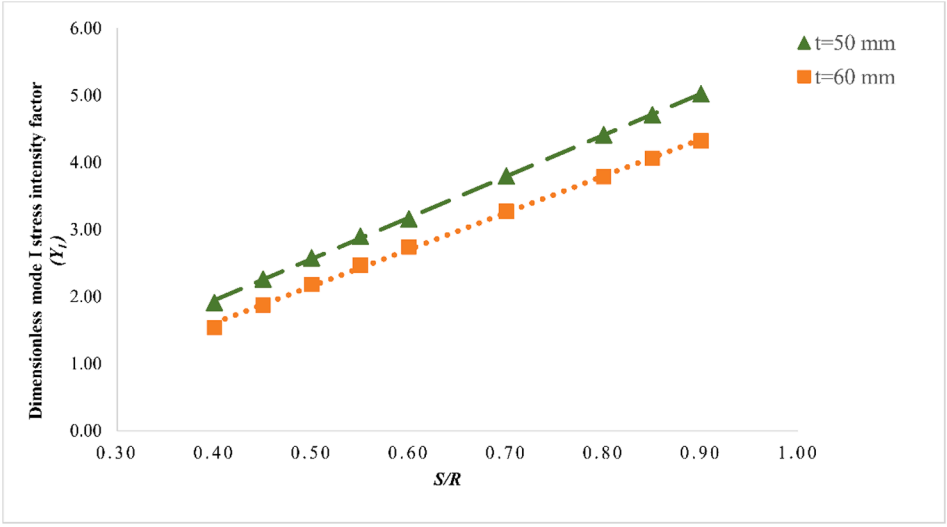

Fig. 5. Y_I versus S/R for two different disc thicknesses of the SNDB model geometry.

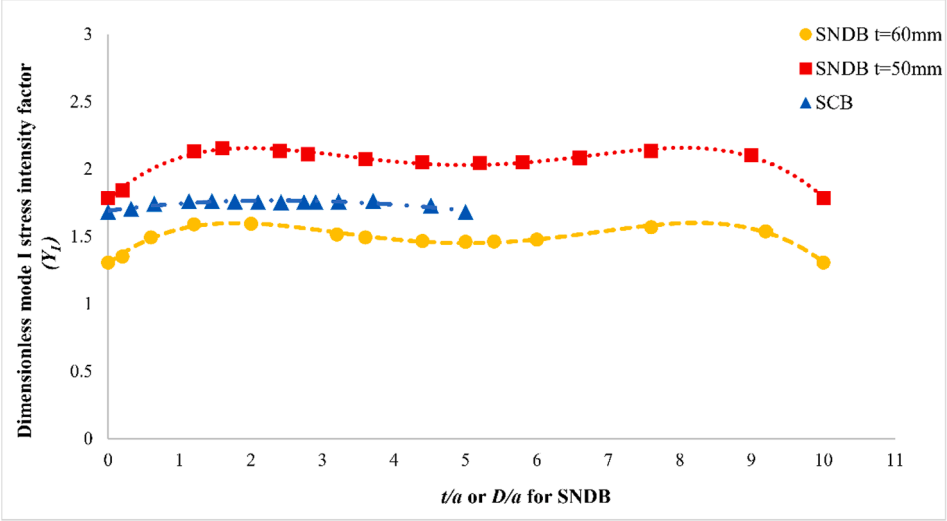

Fig. 6. Variation of Y_I with thickness along the crack front for the third dimension: $2S = 40$ mm.

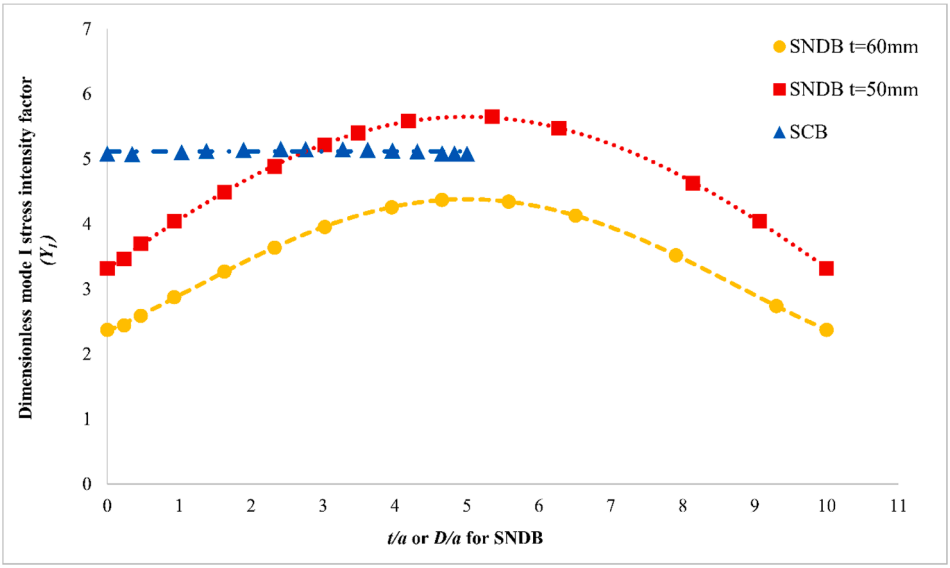

Fig. 7. Variation of Y_I with thickness along the crack front for the third dimension: $2S = 90$ mm.

where K_I is the mode I stress intensity factor and a is the crack length, $\sigma_0 = P/2Dt$ is the disc action stress along the crack front, P is applied load, D is the diameter and t is the thickness of SNDB specimen. Graphical illustration of the Y_I versus span length S/R for $t = 60$ mm and $t = 50$ mm are shown in Fig. 5.

Following the curve fitting process, a linear relation expresses the variation of Y_I with S/R. For estimating the dimensionless mode I stress intensity factor of SNDB model geometries the following equations are proposed for different loading spans:

$$Y_{I(SNDB)} = 6.1604\left(\frac{S}{R}\right) - 0.5192 \text{for} \frac{t}{R} = 1.0 \quad (8)$$

$$Y_{I(SNDB)} = 5.4779\left(\frac{S}{R}\right) - 0.5842 \text{for} \frac{t}{R} = 1.2 \quad (9)$$

Table 3
Material properties of grey colored Ankara Golbasi andesite.

Material Property	Value
Elastic modulus (GPa)	28.3 ± 1.1
Poisson's ratio	0.16 ± 0.01
Uniaxial compressive strength (MPa)	100.8 ± 4.9
Tensile strength (MPa)	8.6 ± 1.1

3.3. Variation of Y_I along thickness for 3D models

State of stress and thus Y_I is expected to vary at the nodes along the thickness of the SCB and SNDB geometry models. Out of plane thickness is 50 mm for the SCB geometry. For the SNDB, variation is to be checked at the crack tip extending all the way along the diameter, which is 100 mm. For this purpose, nodal point data yielding Y_I in the third dimension is presented in Fig. 6 for 40 mm span and in Fig. 7 for 90 mm span cases.

Using a large span like 90 mm ($S/R = 0.90$) increases deviations of Y_I for the SNDB geometry. Modeling program output comes as one single value corresponding to the average of the curved results. As observed in Fig. 6, the deviation has a tendency to disappear as the specimen thickness is increased and the span is decreased. The SCB geometry is

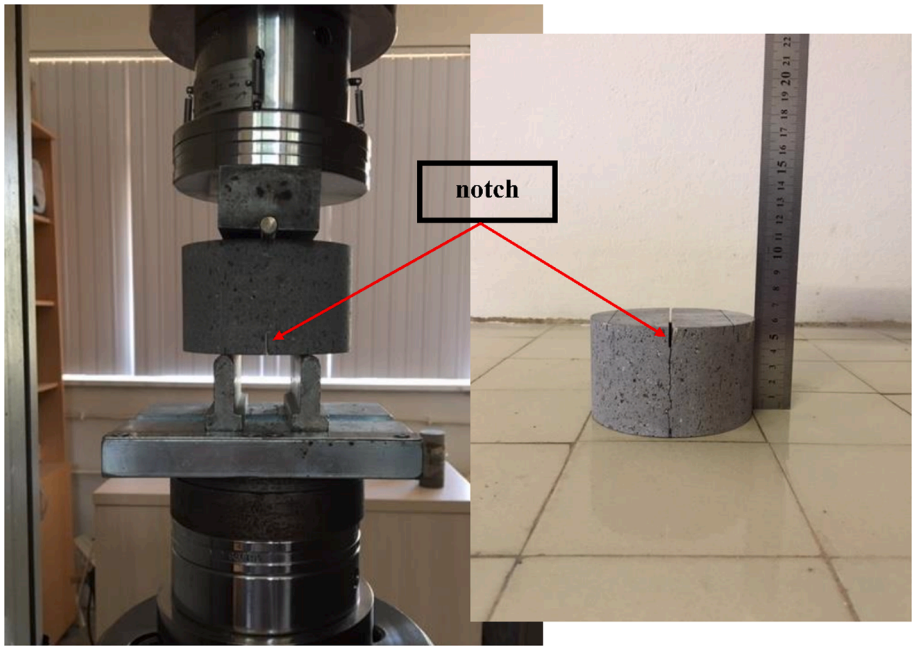

Fig. 8. SNDB specimen during and after test.

essentially plane strain geometry and no significant effect of the third dimension is seen.

4. Experimental work

Circular plate type disc specimen (SNDB) and semi-circular core disc specimen (SCB) were used to assign mode I fracture toughness K_{Ic} of the grey colored Ankara Golbasi andesite. Material properties of the grey colored Ankara Golbasi andesite are summarized in Table 3.

The fracture toughness tests were conducted by stiff servo-controlled MTS 815 Rock Testing System. SNDB and SCB specimens were located between loading platens. The upper platen has an external load cell of 500kN ± 0.25 capacity. Disc and semi-circular disc specimens were loaded with displacement-controlled fashion. The controller unit of the FlexTest 40 provides the actuator to act in a displacement-controlled manner. Loading was applied to the test specimens with a relatively low rate of 0.0003 mm/s. At the end of the test, the maximum load was recorded to calculate the fracture toughness.

SNDB and SCB specimens were tested under three-point bending to find the fracture toughness value under pure mode I. Bending load was provided by rollers that have 8 mm diameter. Bottom support rollers were free to move laterally satisfying the model boundary conditions without any need for frictional constraints. A single roller at the upper surface is for applying the load.

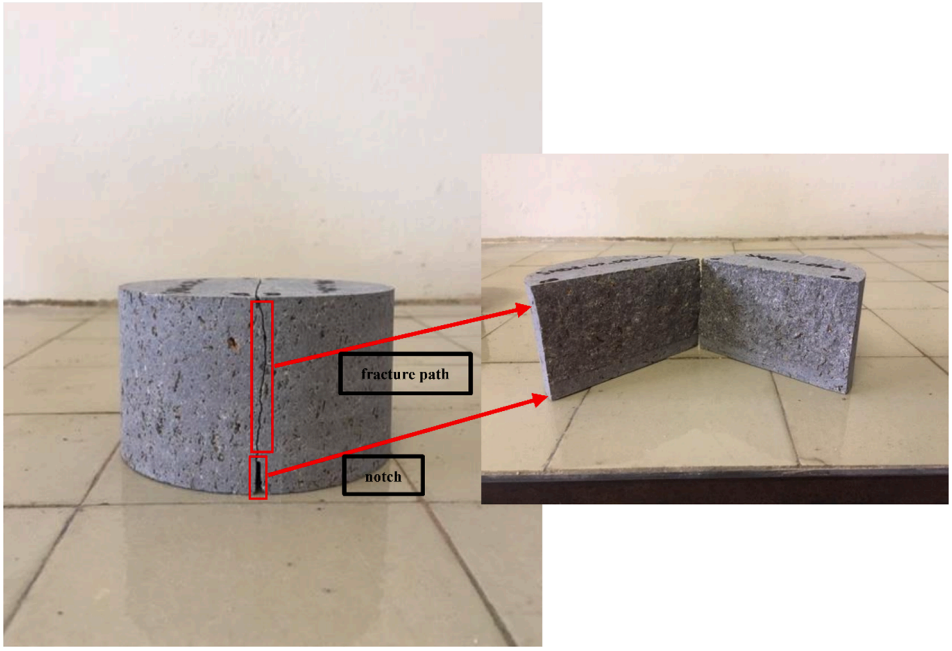

Fig. 9. Notch and fracture path of a typical SNDB specimen.

Table 4
Geometry and results of the SNDB tests with $t = 50$ mm ($t/R = 1$).

Specimen Code	Fracture Load kN	Avg. Fracture Load kN	Span ($2S$) mm	S/R	Mode I Fracture Toughness (K_{Ic}) MPa$\sqrt{m}$	Avg. Mode I Fracture Toughness (K_{Ic}) MPa$\sqrt{m}$
SNDB-50-040-1	35.65		40	0.40	1.20	1.29
SNDB-50-040-2	35.90	38.39	40	0.40	1.21	
SNDB-50-040-3	43.63		40	0.40	1.47	
SNDB-50-045-1	30.28		45	0.45	1.20	1.27
SNDB-50-045-2	26.48		45	0.45	1.06	
SNDB-50-045-3	35.42	32.10	45	0.45	1.41	
SNDB-50-045-4	36.20		45	0.45	1.44	
SNDB-50-050-1	27.86		50	0.50	1.26	1.25
SNDB-50-050-2	28.93	27.69	50	0.50	1.31	
SNDB-50-050-3	26.27		50	0.50	1.19	
SNDB-50-055-1	20.32		55	0.55	1.04	1.23
SNDB-50-055-2	23.57	23.90	55	0.55	1.21	
SNDB-50-055-3	27.80		55	0.55	1.43	
SNDB-50-060-1	20.54		60	0.60	1.14	1.22
SNDB-50-060-2	20.93	21.92	60	0.60	1.16	
SNDB-50-060-3	24.28		60	0.60	1.35	
SNDB-50-070-1	19.23		70	0.70	1.30	1.21
SNDB-50-070-2	17.50	17.86	70	0.70	1.18	
SNDB-50-070-3	16.86		70	0.70	1.14	
SNDB-50-080-1	15.34		80	0.80	1.19	1.20
SNDB-50-080-2	14.32	15.41	80	0.80	1.12	
			80			
SNDB-50-080-3	16.58		80	0.80	1.28	
SNDB-50-085-1	14.80		85	0.85	1.23	1.19
SNDB-50-085-2	15.33	14.36	85	0.85	1.27	
SNDB-50-085-3	12.95		85	0.85	1.08	
SNDB-50-090-1	14.20		90	0.90	1.25	1.18
SNDB-50-090-2	13.69	13.35	90	0.90	1.21	
SNDB-50-090-3	12.17		90	0.90	1.08	
Average ± STD	23.11 ± 8.66				1.23 ± 0.11	

4.1. Specimen preparation for mode I fracture toughness test

Specimen preparation is important process of the rock fracture tests. Attention to the sample preparation process prevents unwanted irregularities and poor results. 100 mm diameter cores were used in overall testing work. Test specimens were subjected to a careful machining process to have accurate dimensions and flat surfaces for both SNDB and SCB specimen geometries. The diamond-impregnated circular saw was utilized for notching processes of both SNDB and SCB specimens. The thickness of the diamond-impregnated circular saw has 0.5 mm.

Table 5
Geometry and results of the SNDB tests with t = 60 mm (t/R = 1.2).

Specimen Code	Fracture Load kN	Avg. Fracture Load kN	Span ($2S$) mm	S/R	Mode I Fracture Toughness (K_{Ic}) MPa$\sqrt{m}$	Avg. Mode I Fracture Toughness (K_{Ic}) MPa$\sqrt{m}$
SNDB-60-040-1	64.50		40	0.40	1.46	1.52
SNDB-60-040-2	63.89	67.28	40	0.40	1.45	
SNDB-60-040-3	73.46		40	0.40	1.66	
SNDB-60-045-1	62.35		45	0.45	1.72	1.50
SNDB-60-045-2	59.46	54.33	45	0.45	1.64	
SNDB-60-045-3	41.19		45	0.45	1.14	
SNDB-60-050-1	47.64		50	0.50	1.53	1.48
SNDB-60-050-2	45.05	46.21	50	0.50	1.45	
SNDB-60-050-3	45.93		50	0.50	1.47	
SNDB-60-055-1	41.91		55	0.55	1.52	1.45
SNDB-60-055-2	38.01	40.14	55	0.55	1.37	
SNDB-60-055-3	40.49		55	0.55	1.47	
SNDB-60-060-1	29.63		60	0.60	1.20	1.41
SNDB-60-060-2	39.83	35.05	60	0.60	1.60	
SNDB-60-060-3	35.69		60	0.60	1.44	
SNDB-60-070-1	24.16		70	0.70	1.16	1.32
SNDB-60-070-2	30.89	27.48	70	0.70	1.49	
SNDB-60-070-3	27.39		70	0.70	1.32	
SNDB-60-080-1	18.54		80	0.80	1.04	1.27
SNDB-60-080-2	28.06	22.76	80	0.80	1.56	
SNDB-60-080-3	26.94		80	0.80	1.50	
SNDB-60-080-4	17.50		80	0.80	0.98	
SNDB-60-085-1	21.56		85	0.85	1.28	1.25
SNDB-60-085-2	20.72	20.97	85	0.85	1.24	
SNDB-60-085-3	20.62		85	0.85	1.22	
SNDB-60-090-1	19.02		90	0.90	1.21	1.21
Average ± STD	37.86 ± 16.25				1.39 ± 0.19	

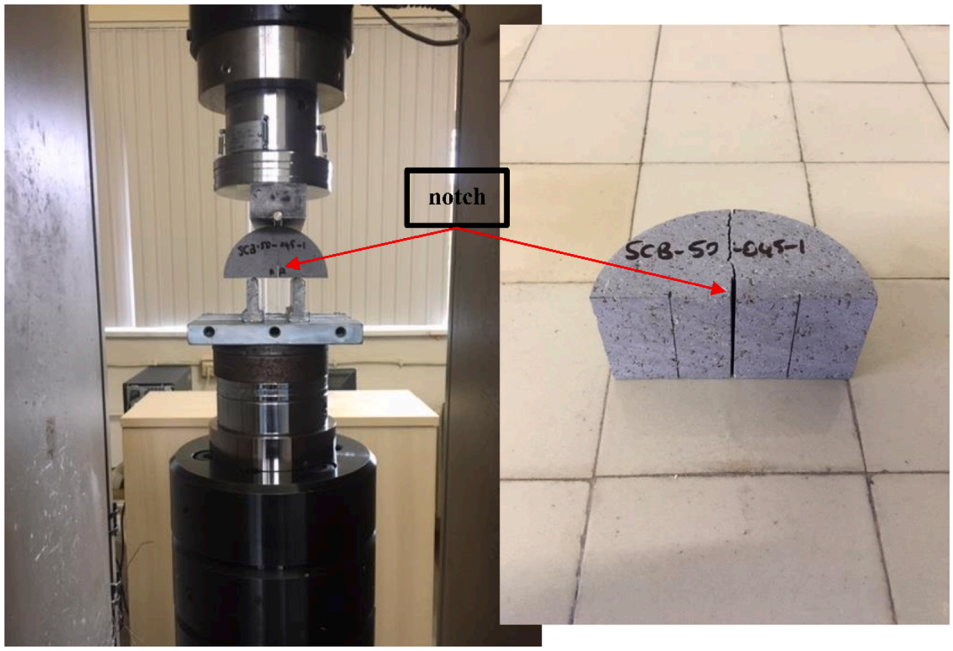

Fig. 10. SCB specimen during and after test.

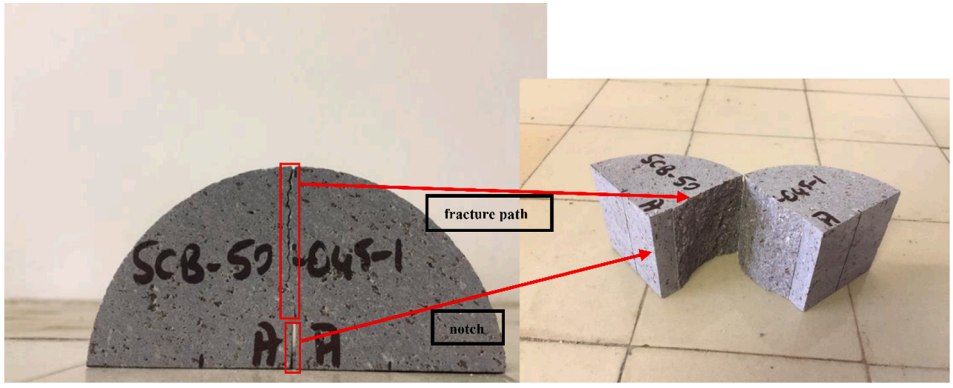

Fig. 11. Notch and fracture path of a typical SCB specimen.

Deviation value of the diamond circular saw machine is about ± 0.2 mm. The notch length value was targeted as 10 mm with a deviation of ± 0.2 mm. In fact, the notch length was kept fixed as 10 mm for both SNDB and SCB specimens. The reason for using a 10 mm crack length (i.e. $a/R = 0.2$) in modeling and testing work is to keep the crack length as small as possible, so that, effect of the outer free boundaries and the loaded boundaries on crack front stress field is minimized. However, in most of the previous research works and even as suggested by the ISRM [6], a higher crack length ratio (typically in the range of 0.3–0.5) is often considered for the SCB specimen. Hence, one of the aims of the current research was to investigate the possible effect of such small crack length ratios on the fracture behavior of rock materials.

4.2. Testing work with SNDB specimen

With SNDB geometry, specimens with two different circular disc thicknesses of $t = 50$ and 60 mm (i.e. $t/R = 1$ and $t/R = 1.2$) were tested. Three-point bending loads were applied to the discs with nine different span lengths: S/R = 0.40, 0.45, 0.50, 0.55, 0.60, 0.70, 0.80, 0.85 and 0.90. Totally, 54 fracture tests were done with SNDB specimen geometry. Fig. 8 and Fig. 9 show the SNDB specimen during fracture toughness testing under three-point bending.

All fracture test results for the SNDB specimens with 50 mm and 60 mm thickness are given in Tables 4 and 5.

Average mode I fracture toughness (K_{Ic}) of the whole 28 SNDB tests with thickness of 50 mm was found as 1.23 ± 0.11 MPa$\sqrt{m}$. The average mode I fracture toughness (K_{Ic}) of 26 SNDB tests with thickness of 60 mm was 1.39 ± 0.19 MPa$\sqrt{m}$.

4.3. Testing work with SCB specimen

Fracture toughness tests with the SCB geometry were performed on 50 mm thick specimens by keeping $t/R = 1$ for all SCB tests. Specimens were prepared with nine different span lengths S/R = 0.40, 0.45, 0.50, 0.55, 0.60, 0.70, 0.80, 0.85 and 0.90. Totally, 27 fracture tests were done utilizing the SCB specimen geometry. Figs. 10 and 11 show the SCB specimen during fracture toughness testing under three-point bending. All fracture test results for the SCB specimens are given in Table 6. Average mode I fracture toughness (K_{Ic}) of 27 SCB tests was found as 0.93 ± 0.19 MPa$\sqrt{m}$.

5. Results and discussion

Average K_{Ic} results from all of the fracture test results are plotted

Table 6
Geometry and results of the SCB tests.

Specimen Code	Fracture Load kN	Avg. Fracture Load kN	Span (2*S*) mm	*S/R*	Mode I Fracture Toughness (K_{Ic}) MPa$\sqrt{m}$	Avg. Mode I Fracture Toughness (K_{Ic}) MPa$\sqrt{m}$
SCB-50-040-1	19.34		40	0.40	1.24	1.20
SCB-50-040-2	18.53	18.73	40	0.40	1.18	
SCB-50-040-3	18.31		40	0.40	1.17	
SCB-50-045-1	13.34		45	0.45	1.03	1.04
SCB-50-045-2	13.20	13.48	45	0.45	1.02	
SCB-50-045-3	13.90		45	0.45	1.07	
SCB-50-050-1	11.19		50	0.50	1.00	1.03
SCB-50-050-2	11.01	11.58	50	0.50	0.98	
SCB-50-050-3	12.54		50	0.50	1.12	
SCB-50-055-1	12.24		55	0.55	1.24	0.96
SCB-50-055-2	6.52	9.50	55	0.55	0.66	
SCB-50-055-3	9.73		55	0.55	0.99	
SCB-50-060-1	6.86		60	0.60	0.78	0.90
SCB-50-060-2	7.10	7.87	60	0.60	0.81	
SCB-50-060-3	9.65		60	0.60	1.10	
SCB-50-070-1	5.09		70	0.70	0.70	0.88
SCB-50-070-2	6.84	6.37	70	0.70	0.94	
SCB-50-070-3	7.18		70	0.70	0.99	
SCB-50-080-1	4.29		80	0.80	0.70	0.80
SCB-50-080-2	4.57	4.95	80	0.80	0.74	
SCB-50-080-3	5.98		80	0.80	0.97	
SCB-50-085-1	4.90		85	0.85	0.86	0.79
SCB-50-085-2	3.92	4.49	85	0.85	0.69	
SCB-50-085-3	4.64		85	0.85	0.81	
SCB-50-090-1	2.91		90	0.90	0.55	0.73
SCB-50-090-2	4.14	3.89	90	0.90	0.78	
SCB-50-090-3	4.62		90	0.90	0.87	
Average ± STD	8.98 ± 4.83				0.93 ± 0.19	

against span length ratio in Fig. 12 where the spans vary from S/R = 0.40 to 0.90. Each average data point there corresponds to the average of three tests with the particular geometry. Fitted curves are attached to the data points in this figure.

The measured fracture toughness changes with the thickness of the SNDB specimen. Average mode I fracture toughness of all SNDB tests with thicknesses of 60 and 50 mm were 1.39 ± 0.19 MPa$\sqrt{m}$ and 1.23 ± 0.11 MPa$\sqrt{m}$, respectively. K_{Ic} of the SNDB specimen for t = 60 mm is about 13% higher than K_{Ic} of the SNDB specimen for t = 50 mm. This difference for 60 mm and 50 mm disc tests gets larger for smaller spans such as S/R = 0.40.

Effect of the loading span on mode I fracture toughness for tests with both SNDB and SCB geometries is clearly observed in overall results. Among all tests, the highest average K_{Ic} is 1.52 MPa$\sqrt{m}$ for 60 mm thick SNDB specimen geometry with the smallest span of S/R = 0.40. For this thickness group, the lowest value is 1.21 MPa$\sqrt{m}$ for tests with span of S/R = 0.90. For t = 50 mm group, again the highest average K_{Ic} is 1.29 MPa$\sqrt{m}$ for the smallest span represented by S/R = 0.40. With span of S/R = 0.90, the lowest value is 1.18 MPa$\sqrt{m}$ for 50 mm thickness group. The corresponding value of K_{Ic} for the SNDB specimen with t = 60 mm decreases by about 26% when span is increased from S/R = 0.40 to 0.90. Similarly, the K_{Ic} of SNDB specimen for t = 50 mm decreases by about 10% when span is increased from S/R = 0.40 to 0.90.

Average mode I fracture toughness value for all SCB specimens is obtained as 0.93 ± 0.19 MPa$\sqrt{m}$, regardless of span. The average K_{Ic} measured by the SCB tests is about 50% lower than the average of all SNDB tests with 60 mm thickness, regardless of span. The average K_{Ic} measured by the SCB tests is about 32% lower than the average of all SNDB tests with 50 mm thickness. Effect of span length on K_{Ic} for the tests using well-recognized SCB geometry under three-point bending was clearly identified in the laboratory work.

Regarding the variation of K_{Ic} with the span, a similar but stronger effect is observed for the tests with well-known SCB geometry. Among all SCB tests, the highest average K_{Ic} is 1.20 MPa$\sqrt{m}$. For the SCB tests, the lowest average value is 0.73 MPa$\sqrt{m}$. According to this, K_{Ic} of the SCB specimen decreases by around 64% when span length is increased from S/R = 0.40 to 0.90.

Increasing the thickness of the SNDB disc specimen geometry has an effect on the fracture toughness value such that K_{Ic} increases with the disc thickness. This enhancement is much higher for the tests with lower S/R of three-point bending load configuration. For larger S/R, the thickness effect gets more dominant resulting in lower K_{Ic} values. For the SCB results, the same trend exists in a stronger manner. Another important finding is that the SCB results are lower than the results of SNDB tests.

In Fig. 12, the data points around the trend curve of SCB tests show larger scatter compared to the SNDB results. The trend line fits yield better fitting qualities for the results of SNDB tests. Fitted cubic polynomial for the SNDB data of t = 60 mm disc geometry has the best fitting quality with R^2 = 0.99, although cubic polynomial fits for the SCB and t = 50 mm thick SNDB data also reach high R^2 values around 0.99. Polynomial function of third-degree $K_{Ic} = 2.45(S/R)^3 – 4.81(S/R)^2 + 2.39(S/R) + 1.18$ results as the best fit between mode I fracture toughness (K_{Ic}) and span (S/R) for 60 mm thick SNDB specimens in Fig. 12. The average maximum and minimum K_{Ic} can be obtained by using first derivative test. A second-degree polynomial function is obtained after taking the first derivative of the polynomial function of degree three. The two different critical points are acquired from the first derivative operation. These critical points are obtained at S/R = 0.33 and 0.98.

The polynomial of degree three for the test results of 60 mm thick SNDB specimen test has a maximum value of K_{Ic} = 1.53 MPa$\sqrt{m}$ at the point S/R = 0.33 and has a minimum value of K_{Ic} = 1.20 MPa$\sqrt{m}$ at the point S/R = 0.98, (Fig. 13). The average maximum and the average minimum K_{Ic} obtained from the SNDB laboratory tests, and the predicted ones from polynomial of degree three are quite close. It is interesting to note that average minimum value of K_{Ic} = 1.20 MPa$\sqrt{m}$ is equal to the SCB test data point for the lowest span of S/R = 0.40.

Considering the high quality of the tests, the results, and the fitted trend curves, it can be claimed that the mode I fracture toughness from a three-point bend test approaches to the identified maximum which is K_{Ic} = 1.53 MPa$\sqrt{m}$. As reported in the literature review section, the SCB testing method is commonly preferred by the researchers due to its

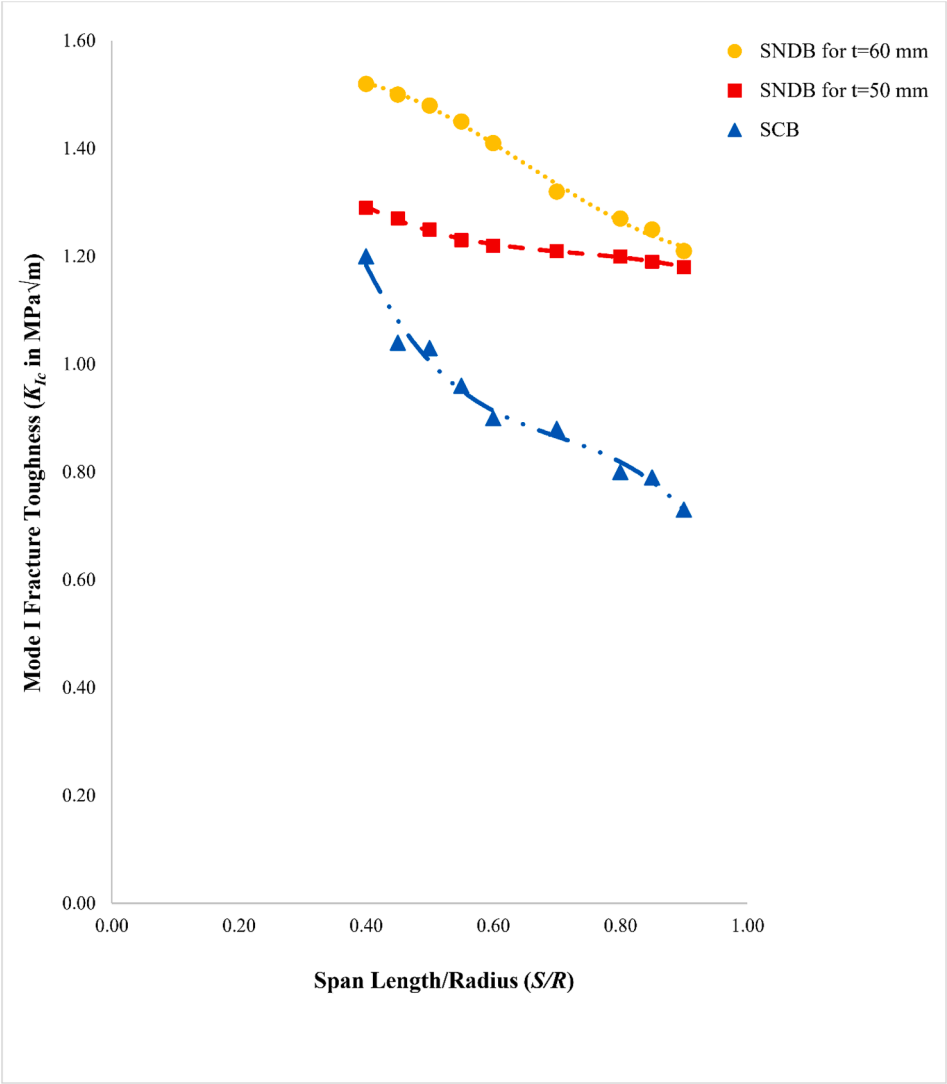

Fig. 12. Average fracture toughness versus S/R for SNDB and SCB specimen geometries.

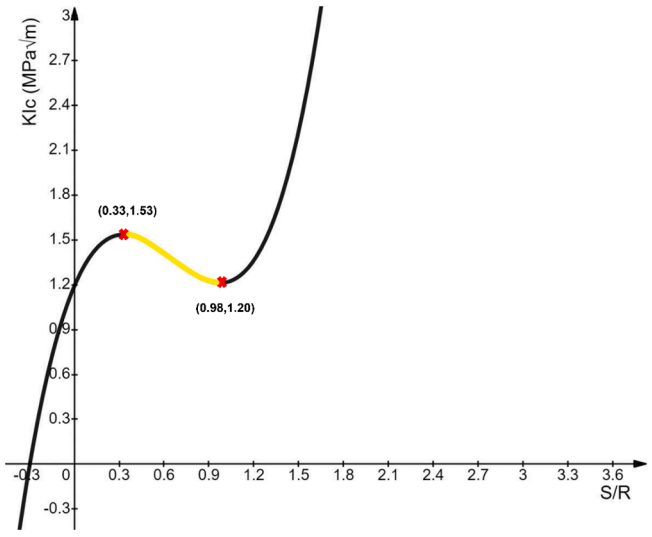

Fig. 13. Graph of the fitted function to the fracture toughness data obtained from the SNDB tests.

simplicity in specimen preparation and easiness of testing procedure. For reaching the size-independent fracture toughness value with the SNDB testing, the boundary effect should be minimized. The influence of boundary decreases with decreasing the span length of loading configuration and increasing the thickness of the SNDB test specimen geometry. To find a K_{Ic} which is affected minimum from boundary influence issue, the SNDB testing should be carried out with a loading configuration having $S/R = 0.40$ or less and a specimen geometry as thick as possible. Using thicknesses like 80 mm ($t/R = 1.6$) or 100 mm ($t/R = 2$) for SNDB test specimens might practically cause problems such as crushing under load and support rollers.

In the literature, span over radius (S/R) has been changed between 0.50 and 0.80 for the SCB method. ISRM suggested a range for SCB test as $0.50 \leq S/R \leq 0.80$ [56]. However, the K_{Ic} value of SCB and CCNSCB tests with specimens having $S/R = 0.3$ was reported recently [57,58]. In our study, successful results for both SNDB and SCB tests were achieved for specimens under three-point bending load with a rather short span of $S/R = 0.40$. In general, K_{Ic} of SNDB tests were about 27 percent greater than K_{Ic} of SCB tests for a span ratio of $S/R = 0.40$.

To investigate the fracture process zone (FPZ), stress analyses are conducted along the paths at the notches of SNDB (straight-notched disc bending) and SCB (semi-circular bending) geometries. Paths covering sufficient number of finite elements ahead of the seam crack are assigned to some ABAQUS models. Average loads are applied to the

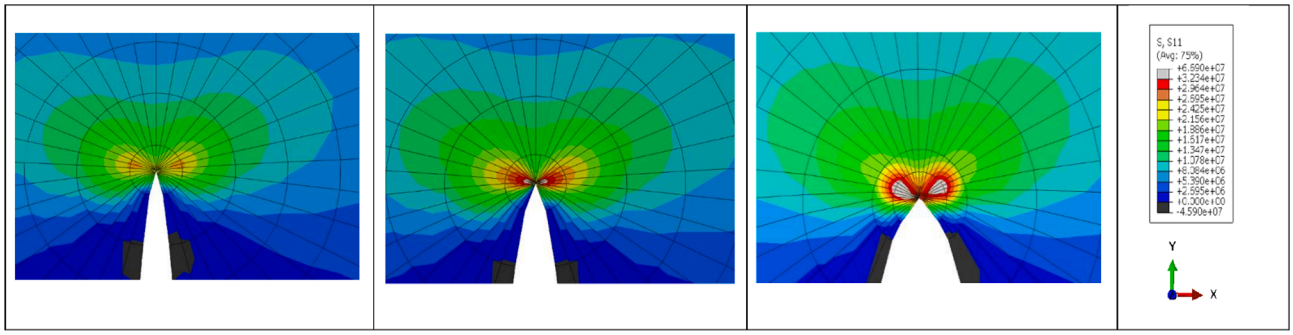

Fig. 14. Normal stress ($S_{11} = \sigma_{xx}$) contour at the crack front for (a) $t = 60$ mm SNDB, (b) $t = 50$ mm SNDB and (c) SCB models.

SNDB and SCB models to simulate and generate the real stress fields of the particular tests. Purpose is to estimate and compare the extent of the possible tensile yield zone for the three cases in consideration. Average loads from the experiments are 19.02 kN for 60 mm thick SNDB specimen, 13.35 kN for 50 mm thick SNDB specimen and 3.89 kN for the SCB specimen, all having the same span of $S/R = 0.90$. These average loads are applied to the SNDB and SCB models to simulate and generate the real stress fields of the particular tests. Stress contours perpendicular to the front of the seam crack (i.e. normal stress component) are plotted in Fig. 14 for the SNDB and SCB model geometries. This is the main stress component leading to the crack opening and propagation. Stress concentration at the crack tip is more intense for the SCB model geometry. The least intense stress concentration is observed for the SNDB geometry of 60 mm thickness.

As stated earlier, the fracture toughness or critical value of mode I stress intensity factor obtained from the SNDB and SCB tests were not the same. In order to explain the mechanism generating the difference in the test results, a theoretical framework is utilized here.

By increasing the level of applied load, the magnitudes of both stress and strain ahead of the crack tip are increased. At critical conditions, very large strains (e.g. infinite stresses/strains) are generated next to the crack tip. Since a real material cannot withstand such loads or deformations, a small zone is created ahead of the crack tip in which the material is damaged within the boundary of this zone and therefore this region no longer sustains any stresses or load carrying capacity. Hence, the crack extension is expected to occur from the boundary of this damage zone. For quasi-brittle materials such as rocks, it is well understood that the crack tip damage mechanism is mainly developed by nucleation and coalescence of micro-cracks such that at the onset of fracture a region surrounding the crack tip is saturated by a large number of micro-cracks. The onset of brittle fracture in rock materials (i.e. initiation of a macro crack inside this damaged zone) takes place when the tangential or tensile stress along the boundary of damage zone attains a critical value that depends on the material resistance against tensile failure. Accordingly based on a strain based fracture model utilized in different research works [34,36,59,60], mode I fracture occurs when the normal or tangential strain (i.e. ε_{yy} or $\varepsilon_{\theta\theta}$) at the boundary of damage zone that is defined by critical distance r_c from the crack tip reaches a critical value $\varepsilon_{\theta\theta c}$. This critical value is considered as constant material property and shows the tensile failure strain at the onset of fracture [59,60]. The normal strain component is written as:

$$\varepsilon_{\theta\theta} = \varepsilon_{yy} = \frac{\sigma_{yy}}{E} - \nu\frac{\sigma_{xx}}{E} - \nu\frac{\sigma_{zz}}{E} \tag{10}$$

where E and ν are the modulus of elasticity and Poisson's ratio, respectively. σ_{xx}, σ_{yy} and σ_{zz} are the stress components in Cartesian system and are written as the following equations for mode I loading condition as outlined by the Williams series expansion [61]:

$$\sigma_{xx} = \frac{K_I}{\sqrt{2\pi r}}\cos\frac{\theta}{2}\left[1 - \sin\frac{\theta}{2}\sin\frac{3\theta}{2}\right] \tag{11}$$

$$\sigma_{yy} = \frac{K_I}{\sqrt{2\pi r}}\cos\frac{\theta}{2}\left[1 + \sin\frac{\theta}{2}\sin\frac{3\theta}{2}\right] \tag{12}$$

$$\sigma_{zz} = \nu(\sigma_{xx} + \sigma_{yy})\text{forplanestrain} \tag{13}$$

Thus by replacing Eqs. (11) to (13) at $\theta = 0°$, into Eq. (10), the following equation is obtained for the normal strain component at plane

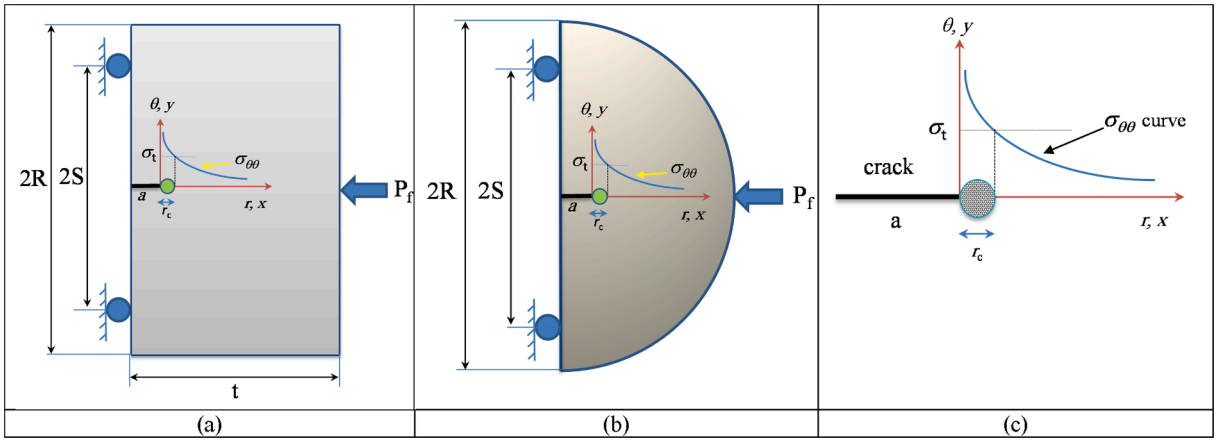

Fig. 15. Schematic representation of tangential stress ($\sigma_{\theta\theta}$) variation versus distance from the crack tip and the corresponding damage zone created ahead of the crack tip for (a) SNDB, (b) (SCB) and (c) zoomed view of crack tip damage zone stress condition.

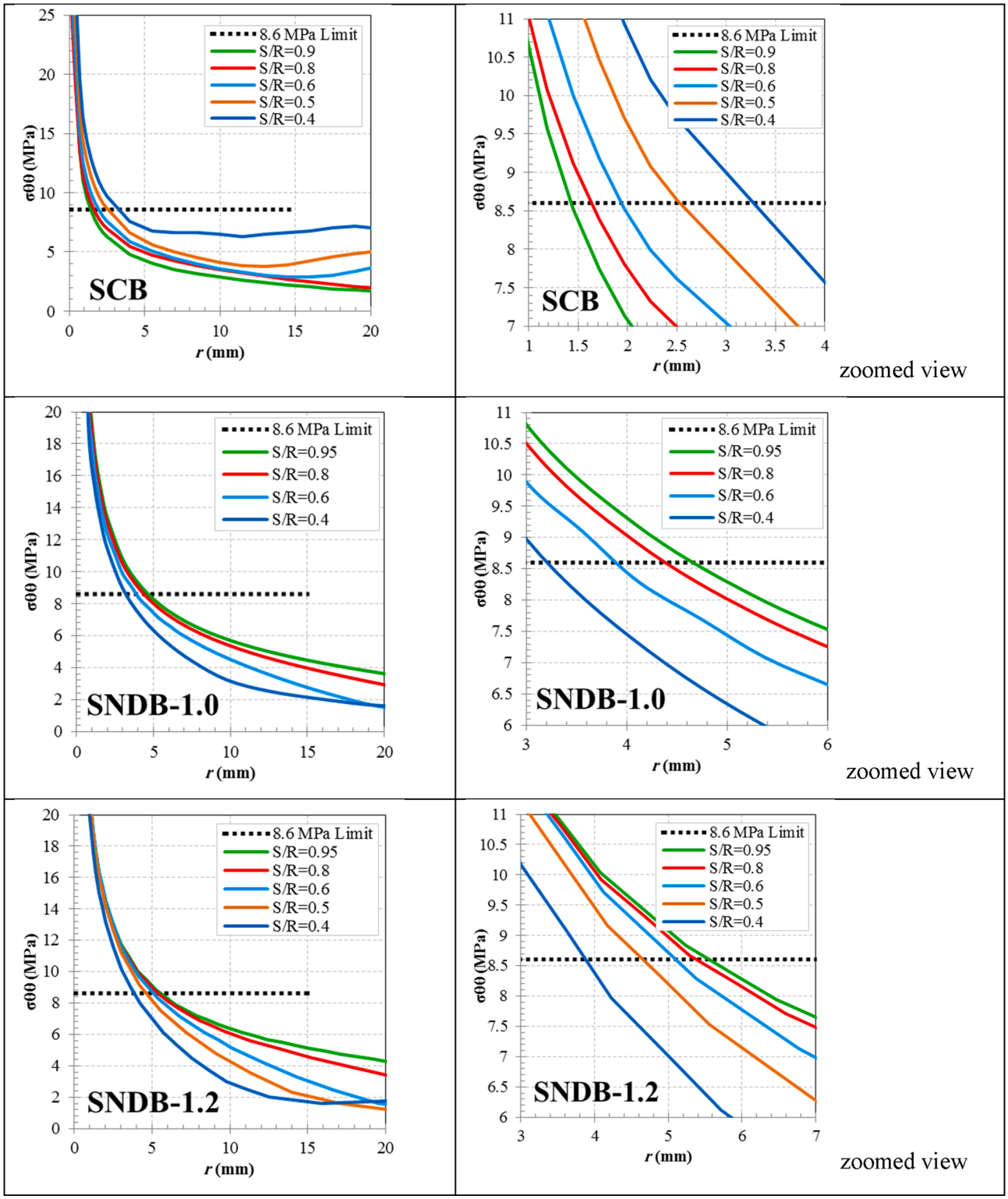

Fig. 16. Corresponding values of critical distance (r_c) determined using the TSC model for the investigated SCB and SNDB samples with different loading spans and made of andesite rock.

strain condition:

$$\varepsilon_{\theta\theta} = \varepsilon_{yy} = \frac{1-\nu-2\nu^2}{E}\frac{K_I}{\sqrt{2\pi r}} \tag{14}$$

At the onset of fracture Eq. (14) can be witten as:

$$\varepsilon_{\theta\theta c} = \frac{1-\nu-2\nu^2}{E}\frac{K_{Ic}}{\sqrt{2\pi r_c}} \tag{15}$$

By assuming $\varepsilon_{\theta\theta c}$ as constant value for the investigated andesite rock material of this research regardless of tested geometry (i.e. SCB or SNDB with two t/R ratios of 1 and 1.2), the following relationships can be written for the mode I critical strains of the tested SCB and SNDB

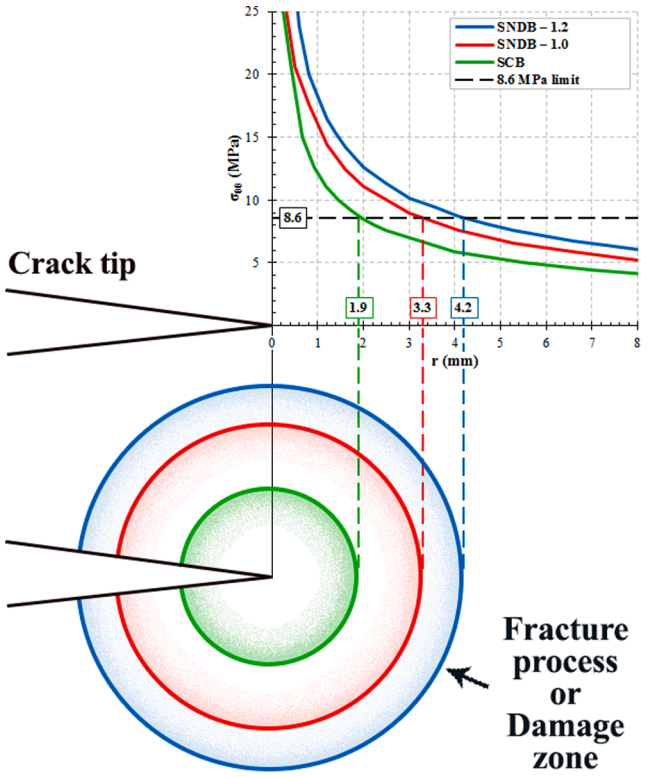

Fig. 17. Average critical distance (r_c) values obtained for the investigated SNDB and SCB samples.

samples:

$$\varepsilon_{\theta\theta c}(SCB) = \varepsilon_{\theta\theta c}(SNDB)|_{t/R=1} = \varepsilon_{\theta\theta c}(SNDB)|_{t/R=1.2} \tag{16}$$

For investigating the validity of Eq. (16), the value of critical distance for the tested mode I samples should also be known. In order to obtain the corresponding value of damage zone or r_c ahead of the crack front in the investigated disc and semi-disc samples of this research, a model called tangential stress contour (TSC) developed by Aliha et al. [62] was utilized. Based on this model, mode I fracture of SNDB and SCB samples subjected to external applied load F, initiates from the boundary of a damage zone in which the maximum tangential stress ($\sigma_{\theta\theta}$) reaches the tensile strength of rock material. By performing a finite element analysis with the same geometry, loading conditions and material properties of the investigated SCB and SNDB samples made of Ankara Golbasi Andesite rock, the corresponding value of critical distance can be determined. To do that, the fracture loads obtained for each sample with different geometries and loading spans are applied to the finite element model and the variations of maximum tangential stress versus the crack tip distance (r) is plotted. The intersection of stress line that equals to the tensile strength threshold of andesite rock (i.e. $\sigma_t = 8.6$ MPa) with the tangential stress curve of each finite element analysis, corresponds to the crack tip damage zone size (as illustrated schematically in Fig. 15 for both SCB and SNDB samples). Fig. 16 shows the critical distance values determined using the TSC method for SNDB and SCB samples. Based on this Figure both specimen geometry (i.e. disc or semi-disc) and loading span (S/R) can affect the value of r_c. This value for the SCB specimen is generally less than two SNDB samples with different thickness values. Moreover, according to the performed analyses the value of r_c increases by increasing the S/R ratio in the SNDB specimen but its value deceases for the SCB sample where the loading span increases. This finding reveals the effect of specimen geometry and constraints on the formation of fracture process zone ahead of the crack tip.

The average values of r_c for three tested geometries determined using the average fracture loads are presented and compared in Fig. 17. By considering these values as representative magnitudes of critical distance in the investigated SNDB and SCB samples, the corresponding value of $\varepsilon_{\theta\theta c}$ for each tested geometry can be determined from:

$$\begin{aligned}
\varepsilon_{\theta\theta\, c}(SCB) &= \frac{1-\nu-2\nu^2}{E}\,\frac{K_{Ic\ (SCB)}}{\sqrt{2\pi\, r_{c\ (SCB)}}} \\
\varepsilon_{\theta\theta\, c}(SNDB-1) &= \frac{1-\nu-2\nu^2}{E}\,\frac{K_{Ic\ (SNDB-1)}}{\sqrt{2\pi\, r_{c\ (SNDB-1)}}} \\
\varepsilon_{\theta\theta\, c}(SNDB-1.2) &= \frac{1-\nu-2\nu^2}{E}\,\frac{K_{Ic\ (SNDB-1.2)}}{\sqrt{2\pi\, r_{c\ (SNDB-1.2)}}}
\end{aligned} \tag{17}$$

The critical tangential strain ratio ($\overline{\varepsilon_{\theta\theta\, c}}$) are defined as following relations for the investigated geometries:

$$\overline{\varepsilon_{\theta\theta\, c}} = \frac{\varepsilon_{\theta\theta\, c}(SCB)}{\varepsilon_{\theta\theta\, c}(SNDB-1)} = \frac{\varepsilon_{\theta\theta\, c}(SCB)}{\varepsilon_{\theta\theta\, c}(SNDB-1.2)} = \frac{\varepsilon_{\theta\theta\, c}(SNDB-1)}{\varepsilon_{\theta\theta\, c}(SNDB-1.2)} \tag{18}$$

By substituting the corresponding values of K_{Ic}, r_c, E and ν for each set of tested SCB and SNDB-1 and SNDB-1.2 samples (given in Tables 3 to 6 and Fig. 17) the corresponding values of right hand sides of Eq. (18) was determined 0.974, 1.06 and 0.991, respectively. This ratio that is very close to unity, demonstrates the validity of Eq. (16) and this fact that although the obtained fracture toughness values were not the same for different test geometries but the critical maximum tangential strain values ($\varepsilon_{\theta\theta\, c}$) of all test samples were nearly the same. It is also finally worth mentioning that the difference between the fracture toughness values obtained from different testing configurations is more noticeable for those materials having greater fracture process zone. Indeed, as demonstrated by some available published works [63,64] the apparent fracture toughness values of materials with small fracture process zone are in good agreement regardless of testing specimen utilized for K_{Ic} measurement.

6. Conclusions

Mode I fracture experiments were conducted on SNDB and SCB specimen geometries. Straight-notched disc bending (SNDB) testing method was preferred due to simplicity of core-based specimen preparation and flexibility to adjust disc specimen thickness for analyzing size effect on the toughness. Span lengths of three-point loading configuration could be varied and optimum span could be found to reach consistent results for mode I fracture toughness. Another three-point bend test, so called semi- circular bending (SCB) test was the choice for comparison purposes. The main results of this research are as follows:

(1) Overall average K_{Ic} of the SNDB specimen decreases around 13% as the specimen thickness decreases from 60 mm to 50 mm. K_{Ic} of the SNDB specimen for $t = 60$ mm decreases by around 26% with increasing the span length ratio as $S/R = 0.40$ to 0.90. The mode I fracture toughness of the SNDB specimen having thickness of 50 mm decreases by around 10% with increasing the span length from $S/R = 0.40$ to 0.90.
(2) The average K_{Ic} of the SCB test is about 50% lower than the average of all SNDB tests with $t = 60$ mm. The average K_{Ic} of the SCB tests is about 32% lower than the average of all SNDB tests with $t = 50$ mm. K_{Ic} of the SCB decreases by around 64%, from 1.20 MPa$\sqrt{m}$ to 0.73 MPa$\sqrt{m}$, with increasing the span length ratio from $S/R = 0.40$ to 0.90. The decreasing trend of K_{Ic} for the SCB geometry with increasing the span is seen to be stronger than the SNDB geometry.
(3) Results of fracture toughness tests are presented for a rather small span of $S/R = 0.40$. In spite of applying the load with such a small span, successful results were obtained without crushing the beam samples under the loading and support rollers. The size independent fracture toughness value of the Ankara Golbasi andesite

is estimated about 1.53 MPa$\sqrt{m}$, based on data processing of the test results for the SNDB geometry. This estimation is justified by stress distribution analyses at the crack front of the test specimen geometries used.

(4) Although the critical value of stress intensity factor was dependent on both specimen geometry and loading span, it was shown that the critical value of normal strain ($\varepsilon_{\theta\theta c}$) is constant for all tested disc bend samples with different loading spans and hence this parameter can be considered as material property.

CRediT authorship contribution statement

Levent Tutluoglu: Data curation, Investigation, Resources, Supervision, Project administration, Conceptualization, Formal analysis. **Ceren Karatas Batan:** Visualization, Writing – orginal draft, Formal analysis, Methodology, Resources. **MRM Aliha:** Project administration, Conceptualization, Investigation, Methodology, Writing – review & editing, Supervision.

Declaration of Competing Interest

The authors declare that they have no known competing financial interests or personal relationships that could have appeared to influence the work reported in this paper.

Acknowledgment

The authors would like to thank Mr. Hamid Reza Karimi for his help in preparation of this research work.

References

[1] L.M. Barker, A simplified method for measuring plane strain fracture toughness, Eng. Fract. Mech. 9 (2) (1977) 361–369.
[2] F. Ouchterlony, Suggested methods for determining the fracture toughness of rock, *Int. J. Rock Mech. Min. Sci. Geomech. Abstracts* 25 (2) (1988) 71–96.
[3] D.K. Sheity, A.R. Rosenfield, W.H. Duckworth, Fracture toughness of ceramics measured by a chevron-notch diametral-compression test, J. Am. Ceram. Soc. 68 (12) (1985) C-325–C-327.
[4] M.R.M. Aliha, M.R. Ayatollahi, Rock fracture toughness study using cracked chevron notched Brazilian disc specimen under pure modes I and II loading–A statistical approach, Theor. Appl. Fract. Mech. 69 (2014) 17–25.
[5] K.P. Chong, M.D. Kuruppu, New specimen for fracture toughness determination for rock and other materials, Int. J. Fract. 26 (2) (1984) R59–R62.
[6] M.D. Kuruppu, Y. Obara, M.R. Ayatollahi, K.P. Chong, T. Funatsu, ISRM-suggested method for determining the mode I static fracture toughness using semi-circular bend specimen, Rock Mech. Rock Eng. 47 (1) (2014) 267–274.
[7] Y.X. Zhou, K.W. Xia, X.B. Li, H.B. Li, G.W. Ma, J. Zhao, F. Dai, Suggested methods for determining the dynamic strength parameters and mode-I fracture toughness of rock materials, in: The ISRM Suggested Methods for Rock Characterization, Testing and Monitoring: 2007-2014, Springer, Cham, 2011, pp. 35–44.
[8] Z. Zhao, H. Wang, Z. Cui, F. Zhao, T. Tang, W. Han, X. Wang, Experimental study on Mode-I fracture toughness using Chevron Straight-notched Semi-circular Bend (CSNSCB) method, Theor. Appl. Fract. Mech. 116 (2021) 103093, https://doi.org/10.1016/j.tafmec.2021.103093.
[9] E. Mahdavi, M.R.M. Aliha, B. Bahrami, M.R. Ayatollahi, Comprehensive data for stress intensity factor and critical crack length in chevron notched semi-circular bend specimen subjected to tensile type fracture mode, Theor. Appl. Fract. Mech. 106 (2020) 102466, https://doi.org/10.1016/j.tafmec.2019.102466.
[10] M. Nejati, A. Aminzadeh, T. Driesner, M.O. Saar, On the directional dependency of Mode I fracture toughness in anisotropic rocks, Theor. Appl. Fract. Mech. 107 (2020) 102494, https://doi.org/10.1016/j.tafmec.2020.102494.
[11] M. Sangsefidi, J. Akbardoost, A.R. Zhaleh, Assessment of mode I fracture of rock-type sharp V-notched samples considering the size effect, Theor. Appl. Fract. Mech. 116 (2021) 103136, https://doi.org/10.1016/j.tafmec.2021.103136.
[12] H.R. Karimi, M.R.M. Aliha, Statistical assessment on relationship between fracture parameters of plain and fiber reinforced polymer concrete materials, Compos. Commun. 28 (2021) 100969, https://doi.org/10.1016/j.coco.2021.100969.
[13] M.R.M. Aliha, H.R. Karimi, M. Abedi, The role of mix design and short glass fiber content on mode-I cracking characteristics of polymer concrete, Constr. Build. Mater. 317 (2022) 126139, https://doi.org/10.1016/j.conbuildmat.2021.126139.
[14] J. He, L. Liu, H. Yang, M.R.M. Aliha, H.R. Karimi, Contribution of interface fracture mechanism on fracture propagation trajectory of heterogeneous asphalt composites, Appl. Sci. 11 (7) (2021) 3013.
[15] D. Yang, H.R. Karimi, M.R.M. Aliha, Comparison of testing method effects on cracking resistance of asphalt concrete mixtures, Appl. Sci. 11 (11) (2021) 5094.
[16] L. Tutluoglu, C. Keles, Mode I fracture toughness determination with straight notched disk bending method, Int. J. Rock Mech. Min. Sci. 48 (8) (2011) 1248–1261.
[17] M.-D. Wei, F. Dai, N.-W. Xu, Y.i. Liu, T. Zhao, A novel chevron notched short rod bend method for measuring the mode I fracture toughness of rocks, Eng. Fract. Mech. 190 (2018) 1–15.
[18] M.R.M. Aliha, A. Bahmani, S.h. Akhondi, Numerical analysis of a new mixed mode I/III fracture test specimen, Eng. Fract. Mech. 134 (2015) 95–110.
[19] M.R.M. Aliha, A. Bahmani, S.h. Akhondi, Determination of mode III fracture toughness for different materials using a new designed test configuration, Mater. Des. 86 (2015) 863–871.
[20] M.R. Eghbali, M. Fallah Tafti, M.R.M. Aliha, H. Motamedi, The effect of ENDB specimen geometry on mode I fracture toughness and fracture energy of HMA and SMA mixtures at low temperatures, Eng. Fract. Mech. 216 (2019) 106496, https://doi.org/10.1016/j.engfracmech.2019.106496.
[21] P.J. Haghighatpour, M.R.M. Aliha, Assessment of freezing and thawing cycle (FTC) effects on mixed mode I/III fracture toughness and work of fracture of HMA asphalt mixtures, Theor. Appl. Fract. Mech. 118 (2022) 103261, https://doi.org/10.1016/j.tafmec.2022.103261.
[22] P.J. Haghighatpour, M.R.M. Aliha, Effect of Marshall and gyratory compaction methods on cracking characteristics of hot mix asphalt concrete materials under all three basic modes of fracture, Theor. Appl. Fract. Mech. 117 (2022), 103207.
[23] A. Bahmani, M.R.M. Aliha, M. Jebalbarezi Sarbijan, S.S. Mousavi, An extended edge-notched disc bend (ENDB) specimen for mixed-mode I+ II fracture assessments, Int. J. Solids Struct. 193-194 (2020) 239–250.
[24] A. Bahmani, S. Nemati, Fracture resistance of railway ballast rock under tensile and tear loads, Eng. Solid Mech. 9 (3) (2021) 271–280.
[25] S. Najjar, A. Mohammadzadeh Moghaddam, A. Sahaf, M.R.M. Aliha, Low temperature fracture resistance of cement emulsified asphalt mortar under mixed mode I/III loading, Theor. Appl. Fract. Mech. 110 (2020) 102800, https://doi.org/10.1016/j.tafmec.2020.102800.
[26] N. Shahryari, M.R. Keymanesh, M.R.M. Aliha, Specimen type effect on measured low-temperature fracture toughness of asphalt concrete, Fatigue Fract. Eng. Mater. Struct. 44 (2) (2021) 551–567.
[27] A. Bahmani, F. Farahmand, M.R. Janbaz, A.H. Darbandi, H. Ghesmati-Kucheki, M. R.M. Aliha, On the comparison of two mixed-mode I+ III fracture test specimens, Eng. Fract. Mech. 241 (2021), 107434.
[28] M.R.M. Aliha, A. Razmi, A. Mousavi, Fracture study of concrete composites with synthetic fibers additive under modes I and III using ENDB specimen, Constr. Build. Mater. 190 (2018) 612–622.
[29] M.R.M. Aliha, F. Berto, A. Bahmani, S.h. Akhondi, A. Barnoush, Fracture assessment of polymethyl methacrylate using sharp notched disc bend specimens under mixed mode I+ III loading, Phys. Mesomech. 19 (4) (2016) 355–364.
[30] M.R.M. Aliha, S.S. Mousavi, A. Bahmani, E. Linul, L. Marsavina, Crack initiation angles and propagation paths in polyurethane foams under mixed modes I/II and I/III loading, Theor. Appl. Fract. Mech. 101 (2019) 152–161.
[31] A. Bahmani, M.R.M. Aliha, F. Berto, Investigation of fracture toughness for a polycrystalline graphite under combined tensile-tear deformation, Theor. Appl. Fract. Mech. 90 (2017) 53–64.
[32] S. Najjar, A. Mohammadzadeh Moghaddam, A. Sahaf, M.R.M. Aliha, Aging Effect on the Mixed-Mode (I/III) Fracture Toughness of Cement Emulsified Asphalt Composite: Experimental and Statistical Investigation, Eng. Fract. Mech. 264 (2022) 108292, https://doi.org/10.1016/j.engfracmech.2022.108292.
[33] M.R.M. Aliha, M. Sistaninia, D.J. Smith, M.J. Pavier, M.R. Ayatollahi, Geometry effects and statistical analysis of mode I fracture in guiting limestone, Int. J. Rock Mech. Min. Sci. 51 (2012) 128–135.
[34] M.R.M. Aliha, M.J. Sarbijan, A. Bahmani, Fracture toughness determination of modified HMA mixtures with two novel disc shape configurations, Constr. Build. Mater. 155 (2017) 789–799.
[35] M.R.M. Aliha, A. Bahmani, Rock fracture toughness study under mixed mode I/III loading, Rock Mech. Rock Eng. 50 (7) (2017) 1739–1751.
[36] M.R.M. Aliha, E. Mahdavi, M.R. Ayatollahi, Statistical analysis of rock fracture toughness data obtained from different chevron notched and straight cracked mode I specimens, Rock Mech. Rock Eng. 51 (7) (2018) 2095–2114.
[37] M.-D. Wei, F. Dai, N.-W. Xu, T. Zhao, Y.i. Liu, An experimental and theoretical assessment of semi-circular bend specimens with chevron and straight-through notches for mode I fracture toughness testing of rocks, Int. J. Rock Mech. Min. Sci. 99 (2017) 28–38.
[38] M.-D. Wei, F. Dai, Y. Liu, N.-W. Xu, T. Zhao, An experimental and theoretical comparison of CCNBD and CCNSCB specimens for determining mode I fracture toughness of rocks, Fatigue Fract. Eng. Mater. Struct. 41 (5) (2018) 1002–1018.
[39] S.-H. Chang, C.-I. Lee, S. Jeon, Measurement of rock fracture toughness under modes I and II and mixed-mode conditions by using disc-type specimens, Eng. Geol. 66 (1-2) (2002) 79–97.
[40] B.N. Whittaker, R.N. Singh, G. Sun, Rock fracture mechanics, Principles, design and applications, 1992.
[41] P.J. Haghighat Pour, M.R.M. Aliha, M.R. Keymanesh, Evaluating mode I fracture resistance in asphalt mixtures using edge notched disc bend ENDB specimen with different geometrical and environmental conditions, Eng. Fract. Mech. 190 (2018) 245–258.
[42] M.R.M. Aliha, P. Jafari Haghighat Pour, Fracture resistance study for hot mix asphalt mixture under out of plane sliding mode, Eng. Fract. Mech. 238 (2020) 107230, https://doi.org/10.1016/j.engfracmech.2020.107230.
[43] M.R. Mohammad Aliha, H. Ghesmati Kucheki, M.M. Asadi, On the use of different diametral compression cracked disc shape specimens for introducing mode III deformation, Fatigue Fract. Eng. Mater. Struct. 44 (11) (2021) 3135–3151.

[44] M. Wei, F. Dai, Laboratory-scale mixed-mode I/II fracture tests on columnar saline ice, Theor. Appl. Fract. Mech. 114 (2021) 102982, https://doi.org/10.1016/j.tafmec.2021.102982.
[45] J. Tang, X. Chen, F. Dai, M. Wei, Experimental investigation of fracture damage of notched granite beams under cyclic loading using DIC and AE techniques, Fatigue Fract. Eng. Mater. Struct. 43 (7) (2020) 1583–1596.
[46] K.P. Chong, M.D. Kuruppu, J.S. Kuszmaul, Fracture toughness determination of layered materials, Eng. Fract. Mech. 28 (1) (1987) 43–54.
[47] R. Nath Singh, G. Sun, A numerical and experimental investigation for determining fracture toughness of Welsh limestone, Min. Sci. Technol. 10 (1) (1990) 61–70.
[48] K. Khan, N.A. Al-Shayea, Effect of specimen geometry and testing method on mixed mode I-II fracture toughness of a limestone rock from Saudi Arabia, Rock Mech. Rock Eng. 33 (3) (2000) 179–206.
[49] L.N.Y. Wong, T.Y. Guo, W.K. Lam, J.Y.H. Ng, Experimental study of cracking characteristics of Kowloon granite based on three mode I fracture toughness methods, Rock Mech. Rock Eng. 52 (11) (2019) 4217–4235.
[50] J. Bidadi, J. Akbardoost, M.R.M. Aliha, Thickness effect on the mode III fracture resistance and fracture path of rock using ENDB specimens, Fatigue Fract. Eng. Mater. Struct. 43 (2) (2020) 277–291.
[51] H. Du, F. Dai, K. Xia, N. Xu, Y. Xu, Numerical investigation on the dynamic progressive fracture mechanism of cracked chevron notched semi-circular bend specimens in split Hopkinson pressure bar tests, Eng. Fract. Mech. 184 (2017) 202–217.
[52] Y. Xu, F. Dai, N.W. Xu, T. Zhao, Numerical investigation of dynamic rock fracture toughness determination using a semi-circular bend specimen in split Hopkinson pressure bar testing, Rock Mech. Rock Eng. 49 (3) (2016) 731–745.
[53] I.L. Lim, I.W. Johnston, S.K. Choi, J.N. Boland, Fracture testing of a soft rock with semi-circular specimens under three-point bending. Part 1—mode I, Int. J. Rock Mech. Min. Sci. Geomech. Abstracts 31 (3) (1994) 185–197.
[54] J.E. Srawley, Wide range stress intensity factor expressions for ASTM E 399 standard fracture toughness specimens, *Conf. of Am. Soc. for Testing and Mater., Committee E-24* 12 (3) (1976) 475–476.
[55] I.L. Lim, I.W. Johnston, S.K. Choi, Stress intensity factors for semi-circular specimens under three-point bending, Eng. Fract. Mech. 44 (3) (1993) 363–382.
[56] R. Ulusay, J.A. Hudson, Suggested methods prepared by the commission on testing methods, Int. Soc. Rock Mech. 628 (2007).
[57] M. Wei, F. Dai, Y.i. Liu, A. Li, Z. Yan, Influences of loading method and notch type on rock fracture toughness measurements: from the perspectives of T-stress and fracture process zone, Rock Mech. Rock Eng. 54 (9) (2021) 4965–4986.
[58] M.D. Wei, F. Dai, N.W. Xu, Y. Xu, K. Xia, Three-dimensional numerical evaluation of the progressive fracture mechanism of cracked chevron notched semi-circular bend rock specimens, Eng. Fract. Mech. 134 (2015) 286–303.
[59] S.i. Fuan, M.a. Ke, L. Kanghe, L.i. Kun, M.R.M. Aliha, Influence of specimen geometry on mode I fracture toughness of asphalt concrete, Constr. Build. Mater. 276 (2021) 122181, https://doi.org/10.1016/j.conbuildmat.2020.122181.
[60] Y.J. Chao, S. Liu, B.J. Broviak, Brittle fracture: variation of fracture toughness with constraint and crack curving under mode I conditions, Exp. Mech. 41 (3) (2001) 232–241.
[61] M.L. Williams, On the stress distribution at the base of a stationary crack, J. Appl. Mech. 24 (1) (1957) 109–114.
[62] M.R.M. Aliha, S.S. Mousavi, S.M.N. Ghoreishi, Fracture load prediction under mixed mode I+ II using a stress based method for brittle materials tested with the asymmetric four-point bend specimen, Theor. Appl. Fract. Mech. 103 (2019), 102249.
[63] Z.-D. Cui, D.-a. Liu, G.-M. An, B.o. Sun, M. Zhou, F.-Q. Cao, A comparison of two ISRM suggested chevron notched specimens for testing mode-I rock fracture toughness, Int. J. Rock Mech. Min. Sci. 47 (5) (2010) 871–876.
[64] M.-D. Wei, F. Dai, N.-W. Xu, T. Zhao, Stress intensity factors and fracture process zones of ISRM-suggested chevron notched specimens for mode I fracture toughness testing of rocks, Eng. Fract. Mech. 168 (2016) 174–189.